

## Application of *in situ* Mössbauer effect methods for the study of electrochemical reactions in lithium-ion battery electrode materials

R. A. Dunlap\* and Ou Mao

*Department of Physics, Dalhousie University, Halifax, Nova Scotia, Canada B3H 3J5*

J. R. Dahn

*Departments of Physics and Chemistry, Dalhousie University, Halifax, Nova Scotia, Canada B3H 3J5*

(Received 31 August 1998)

A method for investigating electrochemical reactions in a Li-ion cell during discharge and recharge using *in situ*  $^{57}\text{Fe}$  and  $^{119}\text{Sn}$  Mössbauer effect measurements is described. An example of the study of a cell utilizing a  $\text{Sn}_2\text{Fe}$  electrode is described, and is discussed in terms of the results of a conventional *in situ* x-ray diffraction study. It is shown that the x-ray-diffraction method is insensitive for the identification of a number of phases formed in these cells because of their very small crystallite size. The present work demonstrates that Mössbauer effect measurements can readily identify these phases and provide important information about grain size effects. This additional information allows for a much more thorough understanding of the reactions that occur during cell discharge and recharge. [S0163-1829(99)04605-6]

### I. INTRODUCTION

A detailed understanding of the reactions in lithium-ion batteries during the charge-discharge cycle is important for the development of high-capacity electrode materials. Since, in many cases, nanoscopic materials are formed during cell cycling, x-ray-diffraction methods are often not effective for identifying the crystallographic phases formed.<sup>1</sup> Mössbauer effect spectroscopy, however, is more sensitive to local structure than x-ray-diffraction methods and is, therefore, a suitable means for studying these processes. Although some battery electrode materials have been studied by *ex situ* Mössbauer effect measurements (e.g., Refs. 1–3), the utilization of *in situ* studies as described in the present paper provides substantially more useful information.

In the present work we describe the techniques for *in situ* Mössbauer effect spectroscopy of an electrochemical cell. Experimental results for a  $\text{Sn}_2\text{Fe}$  anode are described to illustrate the utility of this method.  $\text{Sn}_2\text{Fe}$  is not only a potentially important new material for use in lithium-ion batteries but also allows for both  $^{57}\text{Fe}$  and  $^{119}\text{Sn}$  Mössbauer effect studies. Results are reported for the first discharge and first recharge of the cell, and are discussed in terms of the results of an x-ray-diffraction study.

### II. EXPERIMENTAL METHODS

$\text{Sn}_2\text{Fe}$  was prepared by arc melting elemental components (2N8 Sn and 3N Fe) followed by annealing at 490 °C in argon for three days. Samples were ball milled using a SPEX Model 8000 Mixer/Mill in order to reduce grain size. Samples were milled under argon in a hardened steel vial for a period of 20 h. Two grams of sample were milled using two 12.7-mm-diameter hardened steel balls leading to a ball to a sample weight ratio of 8:1.

Room-temperature x-ray-diffraction studies were used to determine structural properties of the sample. A Siemens D5000 diffractometer equipped with a Cu target and a dif-

fracted beam monochromator was used for these measurements.

Room-temperature Mössbauer effect measurements were made using a Wissel system II constant acceleration spectrometer. Data were collected using an Ortec ACE multi-channel scaling board. For  $^{57}\text{Fe}$  Mössbauer measurements, a  $\text{Pd}^{57}\text{Co}$  source was used and for  $^{119}\text{Sn}$  measurements a  $\text{Ca}^{119\text{m}}\text{SnO}_3$  source was used. The source and spectrometer had an intrinsic linewidths of 0.22 and 0.78 mm/s for the  $^{57}\text{Fe}$  and  $^{119}\text{Sn}$  experiments, respectively. For  $^{57}\text{Fe}$  measurements the center shift and splitting parameters were calibrated using  $\alpha\text{-Fe}$ . For  $^{119}\text{Sn}$  experiments the velocity scale was calibrated using the peak-to-peak splitting of the outer lines of  $\text{Co}_2\text{MnSn}$  (13.134 mm/s). Sn center shifts are given relative to  $\text{CaSnO}_3$ .

For *in situ* Mössbauer effect measurements the electrode material has been incorporated into a cell based on 2325 coin-type cell hardware. This is illustrated in Fig. 1. Circular holes have been cut in the can and cap in order to accommodate Be windows as illustrated. The Be disks (grade PF-60 from Electrofusion, Fremont, CA) contain a measurable quantity of Fe impurity. For  $^{57}\text{Fe}$  Mössbauer effect measurements a consideration of this fact must be included in the data analysis. Figure 2(a) shows the room-temperature  $^{57}\text{Fe}$  Mössbauer effect spectrum of a Be disk. This spectrum may be described by the combination of a singlet corresponding to isolated dilute Fe in the Be matrix, and a doublet (with a less positive center shift) corresponding to clusters of two or more Fe atoms. This fit is illustrated in the figure. For the purpose of simplifying the data analysis described here, the BeFe component has been described by a single asymmetric doublet, which is statistically equivalent to the fit shown in the figure. Other cell components did not show any Fe contamination, as shown by the lack of absorption in their  $^{57}\text{Fe}$  Mössbauer effect spectra.

For confirmation of the analysis of the fresh *in situ* cell, we have also made an *ex situ*  $^{57}\text{Fe}$  Mössbauer measurement

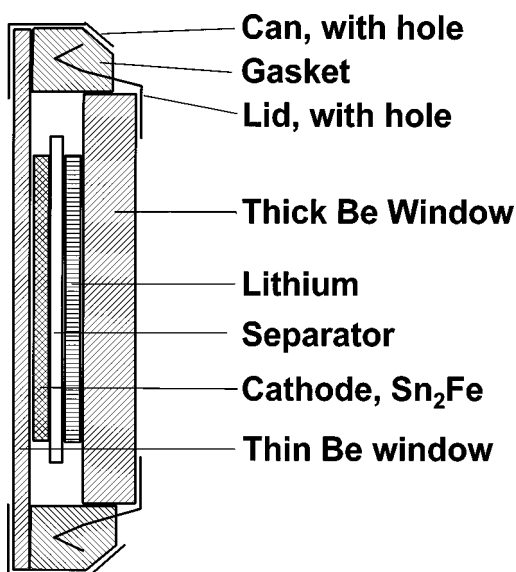


FIG. 1. Design of the cell for *in situ* Mössbauer effect studies.

of the as-milled  $\text{Sn}_2\text{Fe}$  powder, as illustrated in Fig. 2(b). This spectrum is suitably analyzed on the basis of a single Lorentzian singlet with a center shift, as indicated in Table I.  $\text{Sn}_2\text{Fe}$  is antiferromagnetic with a Néel temperature of 377 K and a room-temperature  $^{57}\text{Fe}$  hyperfine field of about 115 kG.<sup>4</sup> However, it has been shown that  $\text{Sn}_2\text{Fe}$  prepared by ball milling is substantially disordered and does not show magnetic order at room temperature. As a result the  $^{57}\text{Fe}$  Mössbauer effect spectrum shows only a singlet.<sup>5</sup> The spectral parameters obtained here are in agreement with this previous work.

The *in situ* Mössbauer effect cell design, as illustrated in Fig. 1, utilizes one thick (1 mm) and one thin (0.25 mm) Be window, and was sealed by a thin bead of Torr Seal (Varian) epoxy after assembly. The electrodes were prepared by coating the mechanically alloyed powder (sieved to  $-325$  mesh) directly onto the thinner Be window. Electrodes contained 85-wt % active powder, 10-wt % Super-S carbon black, and 5-wt % polyvinylidene fluoride. Electrodes were about 1.0 cm in diameter, and contained about 10 mg of  $\text{Sn}_2\text{Fe}$ . The cells used a polypropylene microporous separator, an elec-

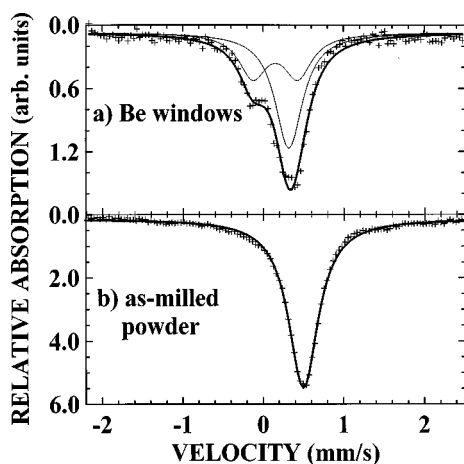


FIG. 2. Room-temperature  $^{57}\text{Fe}$  Mössbauer effect spectra for (a) the Be cell window and (b) ball-milled  $\text{Sn}_2\text{Fe}$  electrode material.

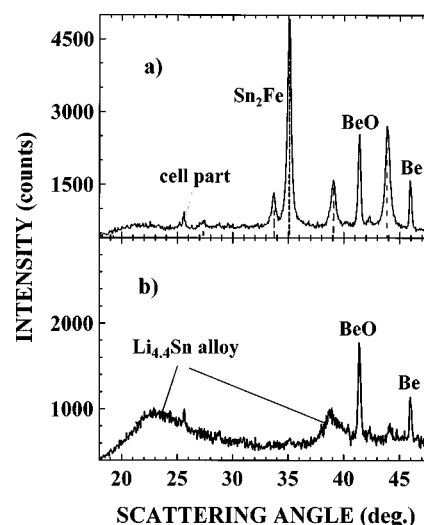


FIG. 3. X-ray-diffraction patterns of  $\text{Sn}_2\text{Fe}$ : (a) fresh cell and (b) at the bottom of the first discharge.

trolyte consisting of 1-M  $\text{LiPF}_6$  dissolved in a 30:70-vol % mixture of ethylene carbonate and diethyl carbonate and a lithium negative electrode.

Charging and discharging currents for *in situ* Mössbauer cells were controlled by a Keithley 220 Programmable Current Source interfaced to a personal computer via a general purpose interface bus (GPIB). Cell voltage was monitored by a Keithley 196 digital volt meter (DVM) and recorded over the GPIB interface. The current was sequentially decreased near the bottom of discharge and near the top of recharge to give reactions time to reach completion. Mössbauer effect spectra were accumulated in the form of scans of approximately 3-h duration throughout the discharge-recharge cycle. The discharge and recharge required about 70–80 h each, yielding a total of 55–60 Mössbauer effect spectra for a complete *in situ* run.

### III. EXPERIMENTAL RESULTS

#### A. X-ray-diffraction studies

X-ray-diffraction patterns of the fresh  $\text{Sn}_2\text{Fe}$  cell and a cell at the bottom of discharge are shown in Fig. 3. Figure 4 compares the x-ray patterns of the fresh cell and the cell at the top of recharge. It is seen in Fig. 3 that the discharge process corresponds to the elimination of the  $\text{Sn}_2\text{Fe}$  peaks and the appearance of peaks due to a lithium-tin alloy. It is known that Sn can accommodate up to 4.4 Li,<sup>6</sup> and that the discharge in these cells corresponds to the reaction<sup>1</sup>



TABLE I.  $^{57}\text{Fe}$  and  $^{119}\text{Sn}$  Mössbauer effect parameters for superparamagnetic  $\text{Sn}_2\text{Fe}$ . For the two probe nuclei the center shifts  $\delta$  are measured relative to room-temperature  $\alpha\text{-Fe}$  and  $\text{CaSnO}_3$ , respectively.  $\Delta$  is the quadrupole splitting.

Mössbauer nucleus	$\delta$ (mm/s)	$\Delta$ (mm/s)
$^{57}\text{Fe}$	0.501	0
$^{119}\text{Sn}$	2.116	0.829

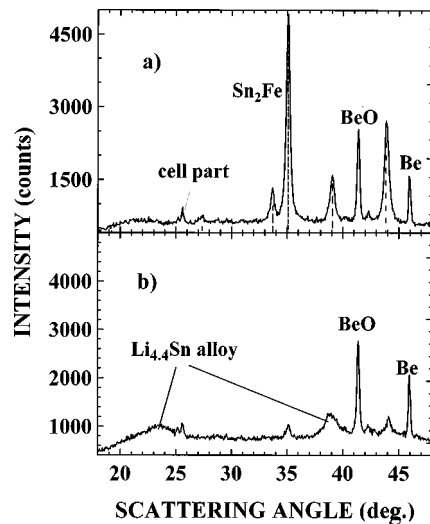


FIG. 4. X-ray-diffraction patterns of Sn<sub>2</sub>Fe: (a) fresh cell and (b) at the top of the first recharge.

This process is seen in the x-ray patterns in Fig. 3. It should be noted as well that the diffraction peaks due to the Li<sub>4.4</sub>Sn phase are quite broad. This was explained in detail by Dahn, Courtney, and Mao<sup>7</sup>

The x-ray patterns, as shown in Fig. 4 for the first recharge, indicate the decrease of the Li<sub>4.4</sub>Sn phase as well as the presence of residual Sn<sub>2</sub>Fe throughout the recharge process. Again, the location of the remaining Fe is not observed, nor is the location of the Sn that is expected to be produced by the delithiation of the Li<sub>4.4</sub>Sn.

### B. <sup>57</sup>Fe Mössbauer effect studies

The voltage curve for the first discharge during which <sup>57</sup>Fe Mössbauer effect spectra were obtained is illustrated in Fig. 5. Selected <sup>57</sup>Fe Mössbauer effect spectra collected during the first discharge of the cell are shown in Fig. 6. At the beginning of the discharge the spectrum, as shown in Fig. 6(a), is well described by the combination of the patterns from the Be window of the cell and the as-prepared Sn<sub>2</sub>Fe electrode material as shown in Figs. 2(a) and 2(b), respectively. This spectrum has been analyzed using the parameters for Fe in Be and Sn<sub>2</sub>Fe, as obtained from the *ex situ* mea-

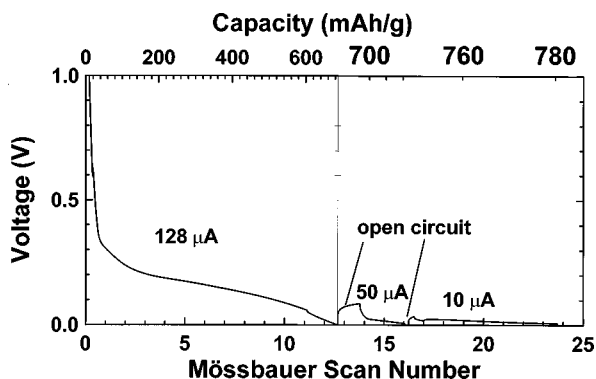


FIG. 5. Voltage vs <sup>57</sup>Fe Mössbauer scan number (bottom axis) and specific capacity (top axis) for the first discharge of the Li/Sn<sub>2</sub>Fe cell. The constant currents are indicated for each portion of the curve.

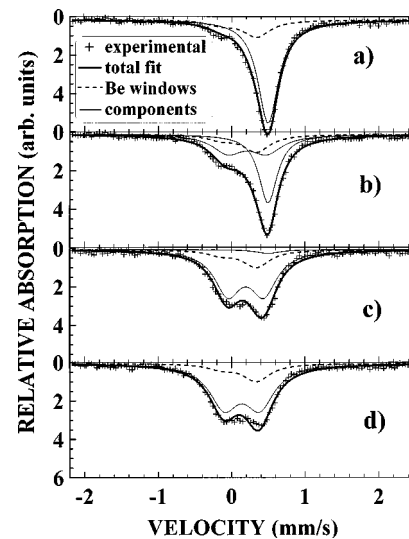


FIG. 6. Selected <sup>57</sup>Fe Mössbauer effect spectra taken during the first discharge: (a) scan 1 (beginning of the discharge), (b) scan 5, (c) scan 12, and (d) scan 24 (bottom of the discharge).

surements; only the relative intensities have been allowed to vary. In the remaining <sup>57</sup>Fe Mössbauer effect spectra of the discharge and recharge of the cell, the Mössbauer parameters including the absolute intensity of the component from Fe in Be have been fixed, as these should not change throughout the cycling of the cell. The series of spectra, as illustrated in Fig. 6, show the gradual reduction in the intensity of the singlet from the Sn<sub>2</sub>Fe phase and the growth of a doublet corresponding to Fe that is produced from the Sn<sub>2</sub>Fe as the Sn reacts with the Li. It has been shown<sup>1,5</sup> that the doublet nature of this component arises because the Fe formed in this process is nanocrystalline. Low-temperature studies<sup>4</sup> have shown that the lack of magnetic splitting results from the fact that these Fe grains are superparamagnetic, with a blocking temperature around 20 K. This implies a grain size of less than about 3 nm.<sup>5,8</sup> The quadrupole splitting results from the large fraction of Fe atoms which occur at the grain boundaries of the nanograin particles.

During the recharge process, the Sn is liberated from Li<sub>4.4</sub>Sn as delithiation occurs. The voltage curve for the recharge during which *in situ* Mössbauer spectra were taken is

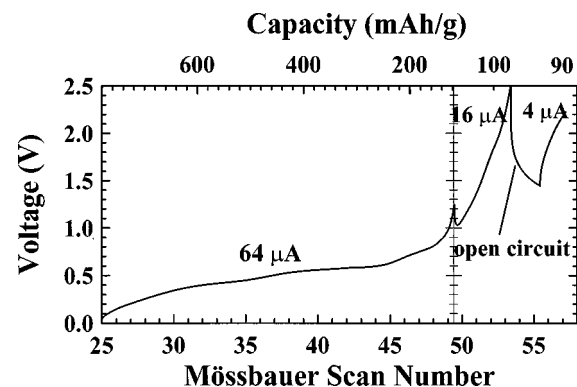


FIG. 7. Voltage vs <sup>57</sup>Fe Mössbauer scan number (bottom axis) and specific capacity (top axis) for the first recharge of the Li/Sn<sub>2</sub>Fe cell. The constant currents are indicated for each portion of the curve.

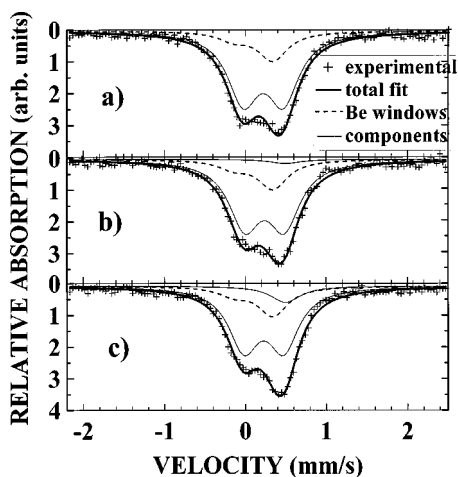


FIG. 8. Selected  $^{57}\text{Fe}$  Mössbauer effect spectra taken during the first recharge: (a) scan 49, (b) scan 51, and (c) scan 57 (top of the recharge).

shown in Fig. 7. Selected Mössbauer spectra taken during the recharge are illustrated in Fig. 8. The Fe, which at the bottom of discharge occurs almost exclusively as nanograined Fe, does not participate significantly in the recharge process until about Mössbauer scan number 49. At this point, as seen in Fig. 8, the singlet corresponding to  $\text{Sn}_2\text{Fe}$  begins to appear. This results from the back reaction of free Sn produced by the delithiation with elemental nanocrystalline Fe. A comparison of the Mössbauer spectra of Fig. 8 with the recharge voltage curve of Fig. 7 shows that the backreaction begins very late in the recharge cycle.

### C. $^{119}\text{Sn}$ Mössbauer effect studies

The voltage curve for the first discharge during which  $^{119}\text{Sn}$  Mössbauer spectra have been accumulated is shown in Fig. 9. Selected  $^{119}\text{Sn}$  Mössbauer effect spectra for the discharge are shown in Fig. 10. The  $^{119}\text{Sn}$  spectrum of the fresh electrode at the beginning of the discharge shows a doublet characteristic of  $\text{Sn}_2\text{Fe}$ . Although the  $^{119}\text{Sn}$  Mössbauer spectrum for antiferromagnetic bulk  $\text{Sn}_2\text{Fe}$  shows a Zeeman splitting, the ball-milled superparamagnetic sample exhibits a quadrupole split doublet, as expected for the  $8h$  Sn sites in the tetragonal  $\text{Sn}_2\text{Fe}$  structure. Parameters for the fit to this

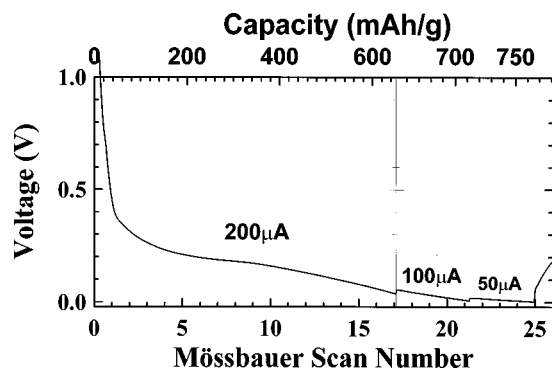


FIG. 9. Voltage vs  $^{119}\text{Sn}$  Mössbauer scan number (bottom axis) and specific capacity (top axis) for the first discharge of the  $\text{Li}/\text{Sn}_2\text{Fe}$  cell. The constant currents are indicated for each portion of the curve.

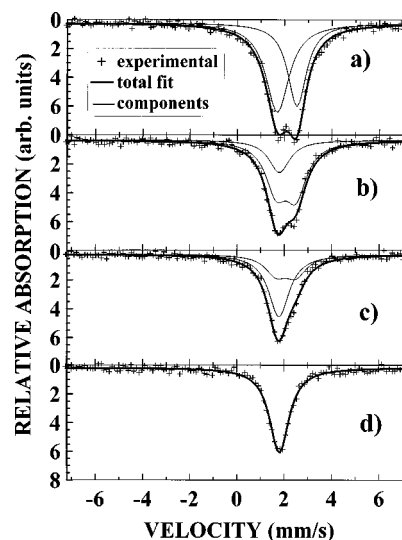


FIG. 10. Selected  $^{119}\text{Sn}$  Mössbauer effect spectra taken during the first discharge: (a) scan 1 (beginning of the discharge), (b) scan 10, (c) scan 15, and (d) scan 25 (bottom of discharge).

doublet are given in Table I. The series of  $^{119}\text{Sn}$  Mössbauer spectra illustrated in Fig. 10 for the discharge shows the gradual decrease of the doublet component and the gradual increase of a singlet component. The center shift of this singlet is 1.80 mm/s, substantially less positive than the shift for metallic Sn (relative to  $\text{CaSnO}_3$ ) of about 2.4 mm/s. This is consistent with the expectations for heavily lithiated Sn as observed in x-ray-diffraction studies.

The voltage curve for the recharge portion of the cycle during which  $^{119}\text{Sn}$  Mössbauer spectra were obtained is shown in Fig. 11. Selected  $^{119}\text{Sn}$  Mössbauer spectra for the recharge are illustrated in Fig. 12. At the beginning of recharge the spectrum is suitably described by a singlet corresponding to heavily lithiated Sn, presumably with a stoichiometry near  $\text{Li}_{4.4}\text{Sn}$ , as expected on the basis of a consideration of the electrochemical reactions. Fairly early in the recharge process a second singlet appears [see Fig. 12(b)], and grows at the expense of the singlet from the heavily lithiated Sn. Initially this second singlet has a center shift of 2.20 mm/s, suggesting that this is lightly lithiated rather than pure Sn. This center shift increases to about 2.40

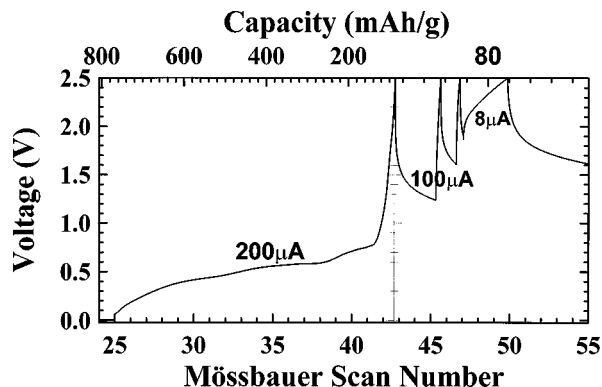


FIG. 11. Voltage vs  $^{119}\text{Sn}$  Mössbauer scan number (bottom axis) and specific capacity (top axis) for the first recharge of the  $\text{Li}/\text{Sn}_2\text{Fe}$  cell. The constant currents are indicated for each portion of the curve.

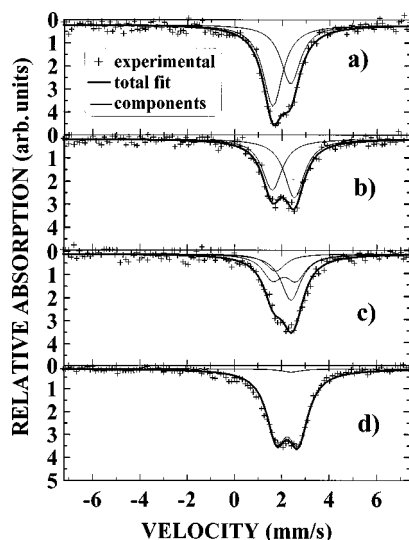


FIG. 12. Selected  $^{119}\text{Sn}$  Mössbauer effect spectra taken during the first recharge: (a) scan 34, (b) scan 38, (c) scan 40, and (d) sum of scans 52–55 (top of the recharge).

mm/s by scan 34, indicating the decrease in the concentration of the Li in this phase. The heavily lithiated Sn component continues to decrease as more Li is removed from the Sn during the discharge (scan 38). Around scan 40 the back reaction of the Sn with Fe to form  $\text{Sn}_2\text{Fe}$  begins, and this produces an additional component to the spectrum. This appears as a doublet with parameters consistent with those observed in the fresh cell. By the end of the recharge the heavily lithiated Sn component has been eliminated, leaving the spectral component from  $\text{Sn}_2\text{Fe}$  and a small component from metallic Sn.

#### IV. DISCUSSION AND CONCLUSIONS

In conjunction with the x-ray-diffraction patterns, the  $^{57}\text{Fe}$  and  $^{119}\text{Sn}$  Mössbauer effect measurements as described above provide a much more comprehensive picture of the reactions that occur in the cell than can be gained from the x-ray studies alone. An overview of what can be learned about the discharge and recharge cycles is provided here. A more detailed quantitative description of the processes involving Fe in these cells was given in Ref. 5.

**Discharge cycle.** The x-ray studies of the discharge cycle indicate the formation of heavily lithiated Sn from  $\text{Sn}_2\text{Fe}$ , as expected on the basis of Eq. (1). The location of the Fe is not seen in these measurements, as the Fe that is produced is of sufficiently small grain size that the x-ray-diffraction peaks cannot be discerned. However, the  $^{57}\text{Fe}$  Mössbauer effect measurements are sensitive to characteristics of the Fe probe nuclei on a much smaller distance scale. These clearly show that the discharge process is described by Eq. (1), that corresponds to the formation of metallic Fe. The characteristic doublet that is observed in these spectra is consistent with our and others' previous investigations of grain size effects in Fe Mössbauer spectra. The  $^{119}\text{Sn}$  Mössbauer spectra reported here show the formation of heavily lithiated Sn during the discharge as is consistent with Eq. (1). The center shift, which is much less positive than that observed in metallic Sn, is consistent with our other investigations.<sup>10</sup>

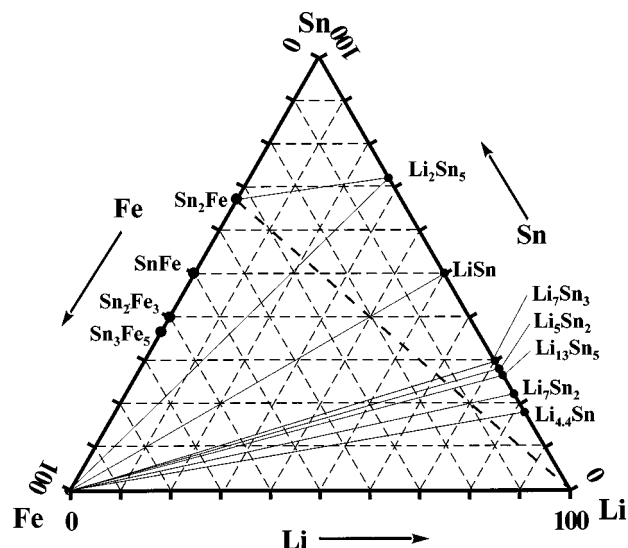


FIG. 13. Proposed Gibbs' composition triangle for the Fe-Sn-Li system.

**Recharge cycle.** The interpretation of the results for the recharge is somewhat more complex than for the discharge. The x-ray studies show a reduction in the heavily lithiated Sn component of the pattern throughout the recharge. Clearly this does not describe the role of most of the Fe in this process, nor does it necessarily account for a substantial fraction of the Sn at the top of the recharge. The processes involved in the recharge can be viewed in terms of the Gibbs' composition triangle for the Fe-Sn-Li system, as shown in Fig. 13. Known intermetallic phases in the Fe-Sn and Sn-Li systems are indicated in the figure.<sup>6</sup> The recharge process corresponds to moving along the broken line in the diagram from the lithium-rich end of the line toward  $\text{Sn}_2\text{Fe}$ . As indicated in Eq. (1) the system at the beginning of recharge consists of a mixture of  $\text{Li}_{4.4}\text{Sn}$  and Fe, and is located at the point where the broken line crosses the  $\text{Li}_{4.4}\text{Sn}$ -Fe line in the figure. In the early stages of the recharge, the system passes through a number of three-phase regions involving two Li-rich Li-Sn intermetallics and Fe. This is followed by three-phase regions involving  $\text{Li}_7\text{Sn}_3$ , LiSn, and Fe and then LiSn,  $\text{Li}_2\text{Sn}_5$ , and Fe. Finally the system enters a three-phase region involving  $\text{Sn}_2\text{Fe}$ ,  $\text{Li}_2\text{Sn}_5$  and Fe. We would, therefore, expect that the recharge process would correspond to a progression from  $\text{Li}_{4.4}\text{Sn} + \text{Fe}$  through a series of heavily lithiated Sn compounds plus iron. When the system crosses the Fe- $\text{Li}_7\text{Sn}_3$  line we expect that lightly lithiated Sn compounds will begin to form, beginning with LiSn, and that these will coexist with the remaining heavily lithiated Li-Sn compounds as well as Fe. When the system crosses the Fe-LiSn line the heavily lithiated compounds should be eliminated. When the system crosses the Fe- $\text{Li}_2\text{Sn}_5$  line, the back reaction of liberated Sn with metallic Fe will begin and will form  $\text{Sn}_2\text{Fe}$ . It is possible that some liberated Sn may be physically isolated from Fe grains, and may be unable to back react. In this case it is expected that metallic Sn in conjunction with Fe or Fe-rich Fe-Sn may also exist. Neither SnFe nor the equilibrium Sn-rich Sn-Fe phases are observed to form in the system after it has crossed into the Fe- $\text{Sn}_2\text{Fe}$ - $\text{Li}_2\text{Sn}_5$  triangle. For this reason the details of the metastable phase diagram, as is appropriate for the recharge-

ing cell, cannot be determined unambiguously. Our investigations<sup>5</sup> suggest an Fe-rich bcc region, but further studies are necessary to clarify the relationship of the various phases in this region.

Our analysis of the recharge on the basis of the Gibbs' triangle is consistent with the results of the <sup>57</sup>Fe and <sup>119</sup>Sn Mössbauer spectra taken in the *in situ* study. As expected, the <sup>57</sup>Fe Mössbauer effect spectrum remains relatively unchanged during most of the recharge until the latter part of the cycle, when the back reaction to form Sn<sub>2</sub>Fe occurs. After the back reaction begins, a singlet component corresponding to Sn<sub>2</sub>Fe appears in addition to the doublet from nanograin Fe. The fact that this occurs fairly late during the recharge is consistent with the explanation based on the Gibbs' triangle in Fig. 13.

The <sup>119</sup>Sn Mössbauer effect spectra can be understood in the context of our Mössbauer effect studies of binary Li-Sn compounds.<sup>10</sup> These indicate that the heavily lithiated compounds (i.e., those from Li<sub>7</sub>Sn<sub>3</sub> to Li<sub>4.4</sub>Sn) have center shifts in the range of about 1.8 mm/s. The lightly lithiated Li-Sn compounds have center shifts which are in the range of 2.2 mm/s to about 2.4 mm/s (for metallic Sn). The appearance and growth of a spectral component near 2.2 mm/s accompanied by a decrease in the intensity of the component near 1.8 mm/s is observed beginning at the point where the system crosses the Fe-Li<sub>7</sub>Sn<sub>3</sub> line. The center shift of this lightly lithiated phase shifts toward more positive values as the average Li content decreases. The Sn<sub>2</sub>Fe component appears and grows at the point where the system crosses the Fe-Li<sub>2</sub>Sn<sub>5</sub> line and the back reaction begins. It is also possible that metallic Sn formed in regions which are isolated from Fe also contribute to the mean center shift observed for the singlet near 2.4 mm/s. The lightly lithiated and/or metallic Sn phase which is observed here is not seen in the x-ray-diffraction measurements shown in Fig. 4, and this presumably is characteristic of the nanocrystalline sized grains of this phase.

Although this would, in principle, seem to account for the identity of all of the phases present during the recharge and at the top of this cycle, the relative proportions of the Mössbauer spectral components need to be justified in terms of the expected reactions illustrated in Fig. 13. From a consideration of the stoichiometries of the phases involved, as well as an analysis of the intensities of the components in the <sup>57</sup>Fe Mössbauer spectra, we would expect that the <sup>119</sup>Sn Mössbauer spectra near the top of recharge would show a fairly substantial component from metallic Sn. However, Fig. 12(d) shows the presence of only a small Sn component. In order to understand this behavior it is important to note that the area of the absorption lines in a Mössbauer spectrum which are due to a certain component in the sample is proportional to both the quantity of the phase present as well as the recoil-free fraction for the Mössbauer probe nuclei in that phase. It is shown here that the recoil-free fraction for Sn nuclei in the metallic Sn phase that is formed during the recharge of these cells is substantially smaller than the recoil-free fraction for Sn in intermetallic Sn<sub>2</sub>Fe. This is in general agreement with the low observed recoil-free fraction for metallic Sn, and results from the lower value of the Debye temperature for the elemental phase compared with Sn compounds.<sup>4,11</sup> This feature is demonstrated by an inspec-

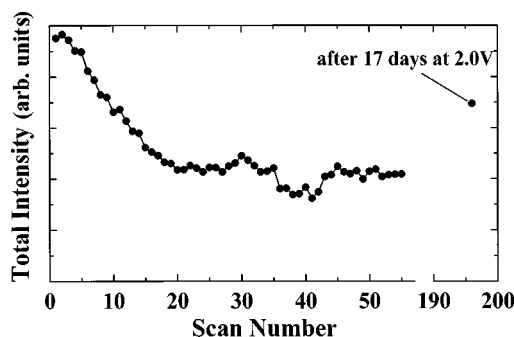


FIG. 14. Total integrated <sup>119</sup>Sn Mössbauer spectral absorption as a function of the scan number. The point at the far right in the graph was obtained after holding the cell at the top of the recharge for 17 days.

tion of the total integrated area of the <sup>119</sup>Sn Mössbauer absorption as a function of scan number during the discharge and recharge, as shown in Fig. 14. At the beginning of the discharge the Sn is contained exclusively in intermetallic Sn<sub>2</sub>Fe, which has a high recoil-free fraction. At the end of the recharge the Sn is distributed between Sn<sub>2</sub>Fe and Sn, which has a low recoil-free fraction. Figure 13 shows the significant decrease in the total spectral area during the first discharge that results from the formation of heavily lithiated Sn, indicating that this phase has a much lower recoil-free fraction than Sn<sub>2</sub>Fe. An additional decrease in recoil-free fraction is observed near scan number 34, where the <sup>119</sup>Sn Mössbauer spectra in Fig. 12 shows the appearance of lightly lithiated Sn from the delithiation of Li<sub>4.4</sub>Sn. The subsequent slight increase in the recoil-free fraction which occurs near scan 40 results from the beginning of the back reaction, which forms Sn<sub>2</sub>Fe, again as seen in Fig. 12. Figure 15 shows the analogous situation for the <sup>57</sup>Fe Mössbauer effect results. It is clear here that there is a relatively small change in the recoil-free fraction of the phases in which the Fe nuclei are contained. This is not unexpected, as we anticipate that the higher Mössbauer transition energy for <sup>119</sup>Sn compared with <sup>57</sup>Fe would make the former probe more sensitive to these effects.

A final point where some apparent discrepancy exists between the x-ray diffraction and the Mössbauer effect results concerns the quantity of Sn<sub>2</sub>Fe present at the top of recharge. Both <sup>57</sup>Fe and <sup>119</sup>Sn Mössbauer effect spectra show that the majority of both Fe and Sn is present in the form of Sn<sub>2</sub>Fe, which results from the back reaction of Sn with Fe. How-

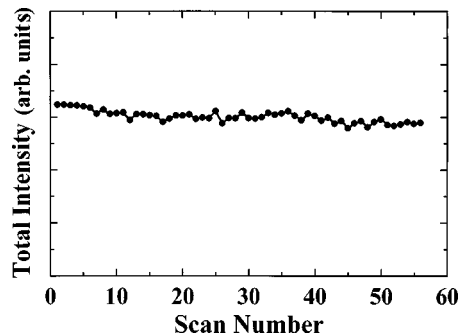


FIG. 15. Total integrated <sup>57</sup>Fe Mössbauer spectral absorption as a function of the scan number.

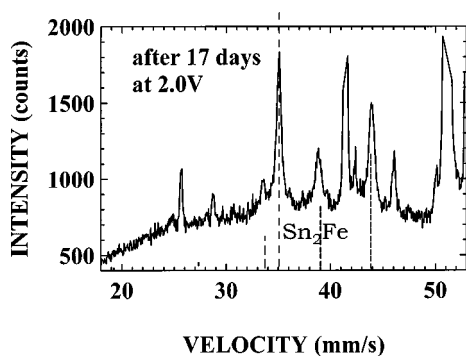


FIG. 16. X-ray diffraction of a cell held at the top of the recharge for 17 days.

ever, the x-ray pattern shown in Fig. 4 suggests that relatively little  $\text{Sn}_2\text{Fe}$  forms during recharge. This difference results from the fact that the  $\text{Sn}_2\text{Fe}$  formed by the back reaction is very finely grained or amorphous, and x-ray diffraction methods are relatively insensitive to the presence of these small grains. This is evidenced by the x-ray pattern of an electrode held at the top of recharge (closed circuit at 2.0 V) for a period of 17 days, as shown in Fig. 16. Holding the cell at this potential for an extended period of time allows the  $\text{Sn}_2\text{Fe}$  grains to grow, and involves the incorporation of additional isolated Sn and Fe into this phase, resulting in a substantial increase in the peak intensity in the x-ray pattern. This interpretation is confirmed by the  $^{119}\text{Sn}$  Mössbauer spectra illustrated in Fig. 17. The spectrum obtained at the top of recharge [Fig. 17(a)] shows a relatively small amount of absorption. This is due to the fact that a substantial quantity of the Sn still exists as metallic Sn with a small recoil-free fraction. This spectrum may be compared with that shown in Fig. 17(b) for the cell held at 2.0 V for 17 days. This is very nearly the same as that for the fresh cell, and indicates that the back reaction has proceeded (almost to completion) during the extended period that the cell has been held at the top of recharge. The changes in the observed recoil-free fraction can be quantified as shown by the data point at the right of the graph in Fig. 14, and are consistent with the above interpretation of the x-ray and Mössbauer data.

The present results have shown that x-ray-diffraction re-

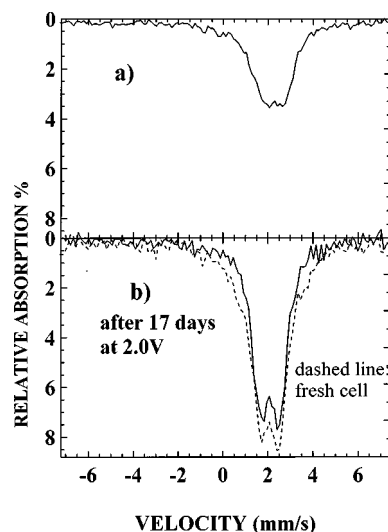


FIG. 17. (a)  $^{119}\text{Sn}$  Mössbauer spectra for the cell at the top of the recharge and (b) a comparison of spectra for the fresh cell (broken line) and the cell held at the top of the recharge (open circuit at 2.0 V) for 17 days (solid line).

sults give an incomplete picture of the processes that occur in the  $\text{Sn}_2\text{Fe}$  electrode during the discharge and recharge cycles. This results from the lack of sensitivity of the x-ray-diffraction technique to nanocrystalline or amorphous materials with grain sizes in the range of a few nm. Complementing these studies with *in situ*  $^{57}\text{Fe}$  and  $^{119}\text{Sn}$  Mössbauer measurements allows for a substantially more thorough understanding of the reactions which occur. The  $\text{Sn}_2\text{Fe}$  system that has been investigated here using this approach has the added advantage of allowing for both  $^{57}\text{Fe}$  and  $^{119}\text{Sn}$  Mössbauer measurements. The ability to identify phases on the basis of centroid shifts and/or quadrupole splittings allows us to provide a complete description of the electrochemical reactions that occur and also, in many cases, to quantify the relative proportions of the phases present and to understand the importance of grain size effects.

#### ACKNOWLEDGMENT

This work was funded by NSERC and 3M Canada Co. under the auspices of the Industrial Research Chair Programme.

\*Author to whom correspondence should be addressed. Electronic address: dunlap@fizz.phys.dal.ca

<sup>1</sup>O. Mao, R. A. Dunlap, and J. R. Dahn, *J. Electrochem. Soc.* **146**, 1405 (1999).

<sup>2</sup>H. Sakai, T. Yamazaki, T. Shigematsu, S. Nakashima, T. Hinomura, and S. Nasu, *Chem. Lett.* **11**, 1101 (1997).

<sup>3</sup>C. H. W. Jones, P. E. Kovacs, and R. D. Sharma, *J. Phys. Chem.* **94**, 832 (1990).

<sup>4</sup>N. N. Greenwood and T. C. Gibb, *Mössbauer Spectroscopy* (Chapman and Hall, London, 1970).

<sup>5</sup>O. Mao, R. A. Dunlap, I. A. Courtney, and J. R. Dahn, *J. Electrochem. Soc.* **145**, 4195 (1998).

<sup>6</sup>M. Hansen, *Constitution of Binary Alloys* (McGraw-Hill, New York, 1989).

<sup>7</sup>J. R. Dahn, I. A. Courtney, and O. Mao, *Solid State Ion.* (to be published).

<sup>8</sup>W. Kundig, H. Bommel, G. Constables, and R. H. Lundquist, *Phys. Rev.* **142**, 327 (1966).

<sup>9</sup>R. D. Shull, J. J. Ritter, and L. J. Swartzendruber, *J. Appl. Phys.* **69**, 5144 (1991).

<sup>10</sup>R. A. Dunlap, D. A. Small, D. D. McNeil, M. N. Obrovac, and J. R. Dahn (unpublished).

<sup>11</sup>C. Hohenemser, *Phys. Rev.* **139**, A185 (1965).